Estuarine, Coastal and Shelf Science 237 (2020) 106659

Contents lists available at ScienceDirect

Estuarine, Coastal and Shelf Science

journal homepage: http://www.elsevier.com/locate/ecss

Shoreline change rates along Samborombón Bay, Río de la Plata estuary, Argentina

Guido L. Bacino [a,b], Walter C. Dragani [a,c,d,*], Jorge O. Codignotto [a,b], Andrés E. Pescio [c,e], Marcelo O. Farenga [f]

[a] CONICET, Consejo Nacional de Investigaciones Científicas y Técnicas. Godoy Cruz 2290 (C1425FQB), Ciudad Autónoma de Buenos Aires, Argentina
[b] Servicio Geológico Minero Argentino (SEGEMAR), Av. General Paz 5445 (B1650WAB), Provincia de Buenos Aires, Argentina
[c] Servicio de Hidrografía Naval, Av. Montes de Oca 2124 (C1270ABV), Ciudad Autónoma de Buenos Aires, Argentina
[d] Instituto Franco-Argentino para el Estudio del Clima y sus Impactos (UMI FAECI/CNRS-CONICET-UBA), Ciudad Universitaria, Pabellón II, 2do. Piso. (C1428EGA) Ciudad Autónoma de Buenos Aires, Argentina
[e] Escuela de Ciencias del Mar, Av. Antártida Argentina 425 (C1104AAD), Ciudad Autónoma de Buenos Aires, Argentina
[f] Instituto de Geología de Costas y del Cuaternario, Facultad de Ciencias Exactas y Naturales, Universidad Nacional de Mar del Plata, Deán Funes 3350, 7600, Mar del Plata, Argentina

ARTICLE INFO

Keywords:
Shoreline change rate
Salt marshes
SWAN model
Conceptual model
Samborombón bay
Río de la Plata

ABSTRACT

Samborombón Bay is an extensive microtidal wetland located in the outer Río de la Plata estuary. Shoreline change rates (erosion or accretion) were quantified at six control areas situated along the bay's coastal area. Digital Shoreline Analysis System 4.3 (DSAS) was used to process aerial photographs and high-resolution satellite images, aiming to quantify shoreline change. A larger 'Total Period' (the last 50 years) and a 'Recent Period' (the last decade approximately) were considered for analyzing shoreline evolution. Erosion and accretion rates increased in five of the six control areas during the last decade. The alongshore (Pl_N) and the incident (Pi) wave energy fluxes were computed from numerical wave simulations. Highest mean annual Pi values were observed at the southern and northern sectors of the bay, and lower values were obtained at the center. Mean annual Pl_N shows a convergent pattern in Samborombón Bay. Some differences between adjacent locations regarding annual mean Pl_N were detected. These differences could generate a slight divergence in Pl_N, leading to mild coastal erosion. Pi presents generally positive trends along the bay. On the contrary, Pl_N only presents a significant trend in the southern part of the bay. Then, while the erosional capability (Pi) is increasing, transport capacity (Pl_N) is quite stable along the coastal area of the bay. Finally, the hydro-sedimentary processes at the coastal area of Samborombón Bay were interpreted by means of a simple conceptual model, which includes internal and external sources of sediments.

1. Introduction

Salt marshes are highly dynamic ecosystems, and their size and boundary stability depend on horizontal and vertical processes. There is extensive evidence around the world that salt marshes are able to keep pace with mean sea level rise (SLR) in the vertical dimension, maintaining their elevation respect to mean sea level, even at high rates of vertical accretion (Kirwan et al., 2016; Leonardi et al., 2016; Schuerch et al., 2016). On the other hand, marshes are rather unstable in the horizontal dimension, representing the principal reason of loss of marsh area in the last few decades (Marani et al., 2011), even in the absence of SLR (Fagherazzi et al., 2013). In this way, the erosion of marsh edges registered in many wetlands around the world, seems to have a significant relationship with the cumulative wave energy and the change in wave climate (Bendoni et al., 2016; Leonardi et al., 2016; Priestas et al., 2015; Schwimmer, 2001; Tommasini et al., 2019; van der Wal and Pye, 2004). Nevertheless other factors could be playing an important role in sediment erodibility at the intermediate scale, like foreshore morphology, and at the local scale, soil and vegetation properties (Wang et al., 2017).

Marsh platforms have been globally studied but lately more attention has been paid to their sustainability threatened by accelerating SLR

* Corresponding author. CONICET, Consejo Nacional de Investigaciones Científicas y Técnicas. Godoy Cruz 2290 (C1425FQB), Ciudad Autónoma de Buenos Aires, Argentina.
E-mail address: dragani@hidro.gov.ar (W.C. Dragani).

https://doi.org/10.1016/j.ecss.2020.106659
Received 27 May 2019; Received in revised form 20 February 2020; Accepted 21 February 2020
Available online 25 February 2020

(FitzGerald and Hughes, 2019). Considering that the mean rate of SLR (which is accelerating) is many times greater than the mean rate at which the marsh platform evolved, it is likely that the marsh area will decrease more rapidly (Fagherazzi et al., 2013), although inland migration was also observed in many wetlands (Anisfeld et al., 2017; Kirwan et al., 2016; Raabe and Stumpf, 2015). It was documented that the erosion of marsh edges and tidal flats in Plum Island Sound and New River Estuaries (USA) represents a significant sediment source to the estuaries and contributes to vertical aggradation of the remaining marsh platform (Currin et al., 2015; Hopkinson et al., 2018). For instance, in Chesapeake Bay (USA) a rapid rate and pattern of marsh edges erosion was previously detected during the last century (Wrayf et al., 1995), predicting that marshland islands will disappear through the 21st century. But, recently, Schieder et al. (2017) found that the rates of marsh erosion and migration uplands are quite similar (~0.5 m/y) at a regional scale in Chesapeake bay (USA). They suggest that sea level rise will lead to a massive drowning of uplands, creating new marshes, compensated at the same time by marshes lost by edge erosion. In Delaware Bay (USA), marsh edge erosion is occurring more rapidly than landward marsh transgression, with a retreat process accelerated in the last periods, causing a net marsh loss (Elsey-Quirk et al., 2019). Moreover, in the Mekong delta (Vietnam) the erosion process was observed in over 50% of its coasts and was linked to a decrease in sediment delivery due to the increase in massive channel bed sand mining within the delta and due to the existing dams (Anthony et al., 2015; Mentaschi et al., 2018). Over the last 40 years, a total marsh area loss of 6% was estimated in Bahía Blanca estuary (Argentina), observed in the replacement of Spartina *perennis* marshes by mudflats (Pratolongo et al., 2013). Coastal Louisiana wetlands are among the most critically threatened, since they have lost approximately 25% of their area in the last century (Couvillion et al., 2017). Venice Lagoon (Italy) experienced a long term net sediment loss due to a decrease in marsh surface (lateral erosion) suffering a decrease in a great extent of salt-marsh, over the last decades (Marani et al., 2011) and century (Tommasini et al., 2019). These last authors observed enlargement and deepening of tidal flat areas, starting in 1932, which promoted an increase in the maximum wave power density. van der Wal and Pye (2004) found that outer estuaries and the wider parts of the inner estuaries of the Greater Thames (England) have experienced erosion in the long term, but they also found evidence of a salt marsh cycle: while the saltmarsh edge retreats, mudflat elevation increases, facilitating the subsequent expansion of *Spartina anglica*, and eventually decreasing the lateral erosion, resulting in salt marsh rejuvenation.

Evident erosive processes in some locations of Samborombón Bay, in the southern coast of the outer Río de la Plata estuary (Fig. 1), were linked to changes and trends in wave climate (Bacino et al., 2019; Codignotto et al., 2012). Positive trends in data series of significant wave height (Hs) and frequency of occurrence (number of cases), particularly in the E direction, were detected along different sites located along the southern coast of the estuary. In addition, a clear linear relationship was found between marsh edge retreat and incident wave energy flux (*Pi*), for three analyzed points within the bay. Even though tides, wind (storm surges) and mean sea level rise play a significant role on the complex hydrodynamic and sedimentary processes in the bay, it was concluded that waves and their changes seem to be the most important agent. This was also observed in many studies of exposed marshes adjacent to open bays and wide tidal channels, indicating that the erosion rate is primarily function of wave power (FitzGerald and Hughes, 2019).

On the contrary, ongoing progradation was detected in some particular coastal marshes located in the central part of Samborombón Bay, via comparison of satellite image series (Lamaro et al., 2009). Drainage improvement in the area by means of canals built during the last century and, consequently, the increase in sediment discharge into the bay, could be a possible explanation of this enlargement (Tosi et al., 2013). In addition, significant vertical growth in the marsh (+2.6 cm/year), higher than the mean SLR, was estimated near the Salado River mouth. The latter suggests that this particular coastal environment would be highly resilient against flooding associated with the different SLR scenarios (Schuerch et al., 2016).

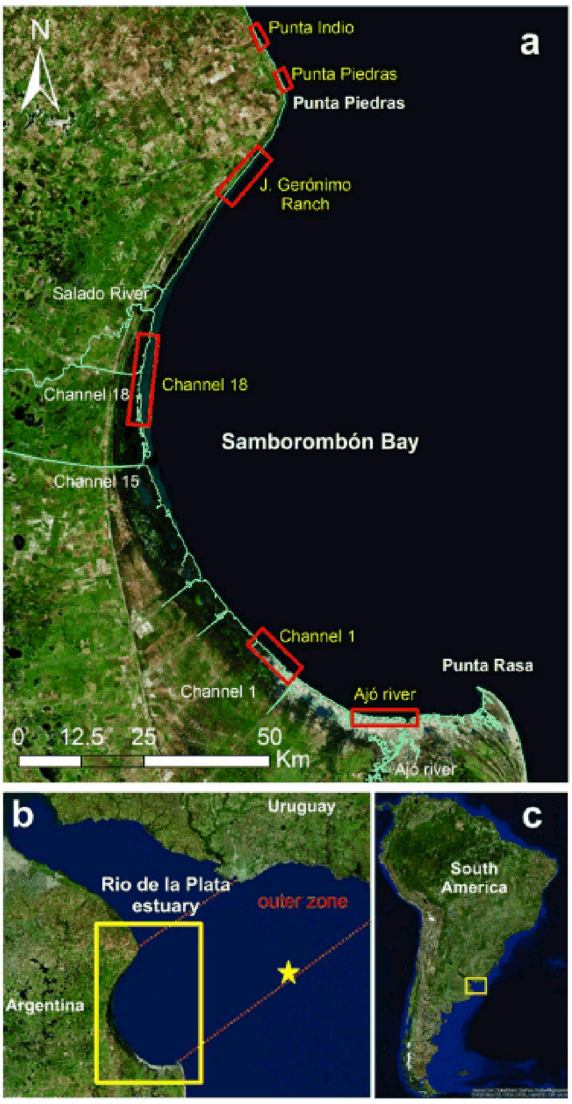

Fig. 1. (a) Samborombón bay, selected areas where shoreline evolution was investigated (red rectangles and names in yellow). (b) Samborombón bay in the outer Río de la Plata context. The yellow star indicates the location of the wave buoy (c) Río de la Plata estuary in South America. (For interpretation of the references to color in this figure legend, the reader is referred to the Web version of this article.)

Samborombón Bay coastal area seems to behave as a complex system where zones of evident progradation and retrogradation could coexist within a delicate sedimentary balance. The aim of this study is to evaluate shoreline change rates at Samborombón Bay. Shoreline time evolution and areas of retrogradation or progradation were investigated at six control areas disposed along the bay, where suitable temporal sequences of satellite images and/or aerial photographs are available. Longshore and incident wave energy fluxes, simulated with Simulating Wave Nearshore (SWAN) model, were also analyzed in order to understand the shoreline change rates. Finally, a simple conceptual model about the sedimentary balance in the coastal area of the bay is proposed.

2. Study area

Samborombón Bay is an extensive microtidal wetland located in the outer Río de la Plata estuary (Fig. 1). Punta Rasa, a sand-spit barrier located in the south tip of the bay, grew in the initial stages of the

Holocene transgression, creating a protected environment which evolved during the last 6000 years into marshes and mud flats (Violante and Cavallotto, 2004). The bay shoreline extends along 140 km where a special ecosystem develops and shelters a variety of species, receiving the RAMSAR site designation in 1997. This wetland is protected by several reserve areas but its main land use is livestock farming, along with mining of shell ridges, which represent the ancient shoreline (Carol et al., 2014).

The Salado and Ajó rivers discharge at the northern and southern sectors of the bay, respectively, draining excess rainfall water from a vast portion of the Buenos Aires province. The lower basin of the Salado River must be dredged frequently and, in addition, artificial channels had to be built to enhance the discharge of rainwater from a large area of the eastern part of Buenos Aires province (Fig. 1.a). The marshlands are approximately 100 m wide at the northern tip of the bay, more than 20 km wide at the southern, they have an average height of 1.5 m above mean sea level, and are composed of low permeability silty-clay sediments (Carol et al., 2014). Marsh vegetation exhibits a strong zonation across the elevation gradient, through their tolerance to flooding and salinity (Isacch et al., 2006). The coastal area in the bay is mainly dominated by *Spartina densiflora*, but *Spartina alterniflora* and *Sarcocornia perennis* can also be found in the lowest intertidal zone.

The shoreline is characterized by a vertical scarp, which exposes the rootmat and the underlying muds mainly controlled by storm surges and waves, as well as bioturbation effects. Codignotto et al. (2012) suggested that the morphodynamics of the marsh edge essentially respond to the effects of the wave action. Waves (sea) in the bay mainly propagate from NE, E, N, and the significant wave height (*Hs*) increases from Punta Piedras to Punta Rasa (Fig. 1) (Bacino et al., 2019).

3. Data and methods

Aerial photographs, satellite images and *in situ* measurements were employed to investigate the shoreline evolution along the bay. In addition, longshore and incident wave energy fluxes were computed from wave parameters simulated with a validated numerical model.

3.1. Aerial photographs and satellite images

A multi-temporal analysis was carried out on available aerial photographs and high-resolution satellite images (Spot7/Quickbird/WorldView2/Pleiades) to quantify the shoreline evolution (retrogradation or progradation) along the bay. Aerial photographs and satellite images cover different time lapses (from 1956 to 2017) depending on the coastal area. For instance, the longest period of available information corresponds to Punta Indio (57 years) and the shortest period (52 years) to J. Gerónimo Ranch and Punta Piedras (Fig. 1.a). Aerial photographs and satellite images were geo-referenced and geometrically transformed using ground control points which were conveniently selected (Hughes et al., 2006). Stable constructions, crossroads or bridges are usually the best elements to define ground control points. However, in coastal marsh areas there are no such elements, therefore, stable trees and landforms in tidal channels or on the terrain were set as control points.

3.2. Shoreline evolution analysis

Determining the coastline could be ambiguous in some marsh areas. For instance, there are some sites where the upper edge of the marsh scarp can be clearly defined differentiating between marsh and mudflat (Schnack, 2010). Nevertheless, there are other areas such as terraces, low-gradient edges or areas with pioneer vegetation at the mudflat, which provide greater difficulty and less accuracy in assessing the coastline. Water level is a very important variable, which plays a critical role in comparing aerial photographs or images obtained from low-slope sites. There are no tidal stations along the coast of Samborombón Bay. The closest tidal station is located southward of the bay, at San Clemente del Tuyú (Fig. 1.a). Sea levels at San Clemente del Tuyú have lags of 3–4 h and 6–7 h with respect to water levels at Channel 1 and Punta Piedras, respectively. Then, the Simplified Empirical Astronomical Tidal (SEAT) model 1.0 (D'Onofrio et al., 2012) was used to assess the tidal level for each image. In general, the escarpment edge can be easily recognized during ordinary tidal level conditions, but the coincidence of high tides and storm surges produces floods, which introduce significant errors in the analysis, particularly at Juan Gerónimo Ranch coastal area. For instance, two satellite images had to be discarded due to atypical floods that occurred in 2003 and 2013 in this area.

The coastline, defined as the upper edge of the scarp, was digitized from scanned paper format images (scale 1:10000) and from digital negatives and satellite images. The uncertainty of the coastline position was estimated following Fletcher et al. (2003), and Genz et al. (2007) who assumed that the errors in the coastline position are normally distributed (Genz et al., 2007).The following uncertainty sources were considered for each coastline: (1) pixel size U_P (m), associated with the image resolution, i.e. any terrain features whose size (less than pixel size) will be undetectable; (2) rectification error U_R (m), which is a measure of the degree of adjustment of the performed transformation (Hughes et al., 2006), and is usually quantified by means of the root mean square error E_{RMS} (Cowart et al., 2010; Fletcher et al., 2003; Genz et al., 2007); (3) digitization uncertainty U_D (m), which is the combination of the error introduced when more than one operator work on the same project (U_{D1}, in m) (Currin et al., 2015; Fletcher et al., 2011) and the manual digitization error (U_{D2}, in m), which accounts for the intrinsic error introduced by the operator. In the present study, U_{D1} was considered equal to zero because only one operator worked on this project and U_{D2} was assumed to be 1 m. Therefore, the total uncertainty U_T (m) can be expressed as:

$$U_T = \sqrt{U_R^2 + U_P^2 + U_{D2}^2} \quad (1)$$

Changes in the coastline rates were quantified by means of the Digital Shoreline Analysis System 4.3 (DSAS) (Himmelstoss, 2009; Thieler et al., 1994), an application developed on ArcGIS 10.0 by the U.S. Geological Survey. DSAS is usually used to quantify rates of shoreline change on transects aligned normal to the coast and regularly spaced along the shore (Thieler et al., 2009). This application is one the most commonly used computational tools for evaluating shoreline changes (see, for example, Fletcher et al., 2003;). The mean endpoint rate (*EPR*, in m/year) was defined as the quotient between the average net shoreline movement on the transects (*NSM*, in m) and the elapsed time between an old (initial) and a recent (final) image (Δt). Analyzed transects along the marsh edge scarp were spaced every 50 m. Even though the linear regression method has been widely used to evaluate shoreline change rates on images, it tends to underestimate these rates in comparison with the *EPR* method (Genz et al., 2007; Thieler et al., 2009).The confidence of the *EPR* method (*ECI*) (Himmelstoss, 2009) can be estimated as:

$$ECI = \frac{\sqrt{U_{Ti}^2 + U_{Tf}^2}}{\Delta t} \quad (2)$$

U_{Ti} and U_{Tf} are the total uncertainty corresponding to the more recent (initial) and the oldest (final) image, respectively. Consequently, the shoreline change rate and its uncertainty can be expressed as $EPR \pm ECI$. Consequently, when shoreline change rate is sufficiently large, i.e. greater than 500 m, and the uncertainty in the positioning is relatively low, the computed change rates are highly reliable. On the contrary, when the uncertainty in positioning is rather high and shoreline change is relatively small, the shoreline change rates become less reliable. In addition, the use of several images distributed during extended periods allow us to distinguish short-term fluctuations (noise) from long-term shoreline changes (Aiello et al., 2013).

3.3. Wave simulations

The SWAN model solves the transport equations for wave action density (Booij et al., 1999), and was used to simulate significant wave height (*Hs*), peak period (*Tp*) and direction (α') in Samborombón Bay. The simulated wave direction ($0 \leq \alpha' < 360°$) indicates where the wave is coming from (0° from the north, 90° from the east, 180° from the south, and so on). Default values were considered for controlling dissipation by depth-induced wave breaking, dissipation by bottom friction, white capping, three wave-wave interaction (triads) and computation of quadruplets. Surface wind data from NCEP/NCAR Reanalysis I (space resolution 1.875° in longitude and 1.905° in latitude) were used to force the simulations (input). These data have been successfully utilized as forcing in several numerical regional studies in the area (Bacino et al., 2019; Codignotto et al., 2012; Dragani et al., 2010; Simionato et al., 2007, 2006; 2005).The bathymetry data used for the SWAN model were obtained combining a depth data set with 1′ x 1′ resolution taken from GEBCO (2003) charts for the continental shelf and nautical charts (SHN, 1999a; 1999b, 1992; 1986).

The computational domain extends from 29.747° to 42.203° S, and from 40.405° to 65.418° W, with a spatial resolution of 22.7 × 20.0 km (100 x 70 grid points). More details about the architecture, implementation, and validation of SWAN model in the study area can be found in Dragani et al. (2008), Martin et al. (2012), and Bacino et al. (2019). Numerical simulations (1971–2018) were validated using *in-situ* wave parameters (1996–2006) and satellite Hs (1991–2017). Computed bias (the difference between observed and simulated mean values), root mean square error and correlation coefficient between *in-situ* (satellite) and simulated Hs were +0.11 m, 0.34 m and 0.70 (−0.04 m, 0.41 m and 0.71), respectively.

3.4. Longshore wave energy flux

The rate of longshore sediment transport (CERC, 1984) is proportional to the alongshore wave energy flux per unit crest (*Pl*), which can be estimated by:

$$Pl = 0.05\ \rho\ g^{3/2}\ H^{5/2}\ (\cos\alpha)^{1/4}\ (\sin 2\alpha) \quad (3)$$

ρ is the water density (equal to 1022.5 kg m^{-3}, Piola and García, 1993), g the acceleration due to gravity (9.86 m s^{-2}), and α the wave angle between the wave crest and the shoreline. The predominant orientation of the shoreline (with respect to a geographic parallel) was estimated from Landsat images (Data SIO, NOAA, U.S. Navy, NGA, GEBCO). Simulated wave direction (α') was transformed to obtain the angle between the direction of wave propagation and a line normal to the coast (α).*Pl* can only flow in two possible directions depending on the sign of the instantaneous value of α, rightward (positive) or leftward (negative), with respect to an observer located at the coast and facing the water. Accordingly, annual net *Pl* (Pl_N, the average of individual rightward and leftward *Pl* in a year) can also flow in a rightward or leftward direction. Details of the estimation of *Pl* along Samborombón Bay coast can be seen in Bacino et al. (2019).

3.5. Incident wave energy flux

If losses or addition of energy are negligible (energy conservation) in the wave propagation from deep/intermediate water to shallow water, the incident wave energy flux per unit crest (*Pi*) at the breaking line can be computed as:

$$Pi = (\rho\ g\ H_s^2\ Cg\ \cos\alpha)\ /\ 8 \quad (4)$$

Hs and α are obtained from the numerical simulation, and group velocity (*Cg*) can be estimated from *Tp* and the local depth by means of the dispersion relation given by the linear wave theory (see, for example, Dean and Dalrymple, 2001).

3.6. Annual rates of marsh edge retreat

Measurements of the cliff retrogradation were carried out at three selected points of the Samborombón Bay coast since January 2010 (Fig. 1.a). Two sites are located at Punta Piedras and Juan Gerónimo Ranch (at the North of the bay) and another at Channel 1 (at the central/South sector of the bay). Control points were fixed very close to the edge of the cliff at each one of the mentioned locations. The distance from the control point to the edge of the cliff is periodically surveyed. These surveys allow the calculation of annual rates of mean marsh edge retreat of 0.66, 1.26 y 0.38 m/year at Channel 1, J. Gerónimo Ranch and Punta Piedras, respectively, which are highly correlated with the simulated *Pi* in the bay (Bacino et al., 2019).

4. Results

Total and recent *NSM* and *EPR* were quantified at six coastal areas of the bay: two small areas at Punta Indio and Punta Piedras, and four relatively large areas located at Juan Gerónimo Ranch, Channel 8, Channel 1, and Ajó River. Images taken from 1964 to 2017 and from 2010 to 2017 were used for estimating the total and recent rates, respectively. In addition, alongshore and incident wave energy fluxes (and their trends) were computed from data series of 39 years long of wave parameters simulated with SWAN model (1979–2018).

4.1. Shoreline change

4.1.1. Punta Indio

Total *NSM* and *EPR* between 1956 and 2013, equal to-188 m and −3.8 ± 0.2 m/year (erosion), respectively, were estimated (Fig. S1). Recent *EPR* was quite similar to the total rate (−3.5 ± 0.9 m/year), with *NSM* equal to −8 m (period: 2010–2013), which is in agreement with the rate obtained by Cellone et al. (2016) who studied the same coastal area using images taken at different times.

4.1.2. Punta Piedras

Lower total *NSM* and *EPR* (-44 m and −0.8 ± 0.4 m/year, respectively) were estimated at Punta Piedras between 1964 and 2016 (Fig. S1). On the contrary, the recent *EPR* (−2.0 ± 0.3 m/year) was a little larger than the total *EPR* (*NSM* = −14 m, period: 2010–2016). It is also a little larger than the annual marsh edge retreat (−0.38 m/year) estimated by Bacino et al. (2019) by means of systematic measurement using control points located at the coast (period: 2010–2015). *EPR* computed for at the closest transect to the control point (20 m far) was −0.72 ± 0.3 m/year.

4.1.3. Juan Gerónimo Ranch

Only three images are available for Juan Gerónimo Ranch area (1964, 2010 and 2016). The analysis carried out in this work allows us to clearly distinguish two different zones (Fig. 2) in this coastal area. At the northern sector (JGN), the total *NSM* and *EPR* were estimated at +35 m and +0.8 ± 0.2 m/year (accretion), respectively, between1964 and 2010. At the southern sector (JGS), total *NSM* and *EPR* were −192 m and −4.2 ± 0.2 m/year (erosion), respectively. On the contrary, negative (erosion) recent *EPR* were estimated in both sectors (period: 2010–2016). *EPR* equal to −0.7 ± 0.5 m/year (*NSM* = −30 m) and −11.6 ± 0.5 m/year (*NSM* = −70 m) were estimated for the northern and southern sectors of Juan Gerónimo Ranch, respectively. Recent *EPR* and *NSM* calculated for the whole area (JGN and JGS) were −8.8 ± 0.5 m/year and −55 m, respectively. This is significantly larger than the annual marsh edge retreat (−1.26 m/year) measured at the southern JGN (2010–2015), near the limit with JGS (Bacino et al., 2019).*EPR* computed for the closest transect to the control point (16 m far) was −1.77 m/year (2010–2016).

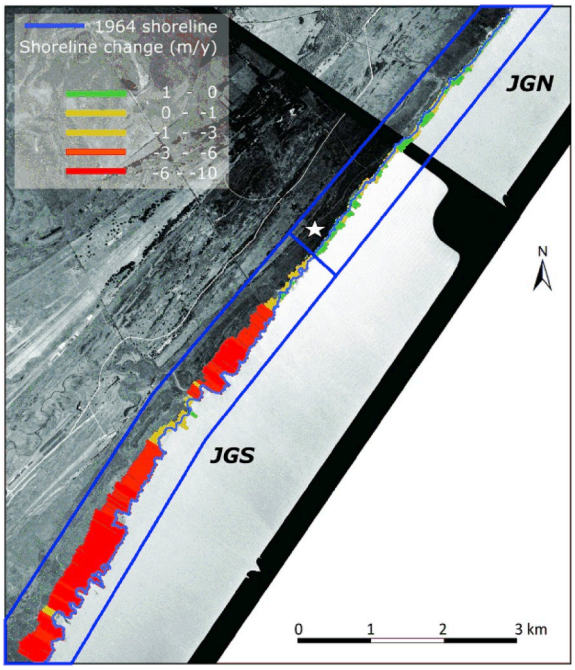

Fig. 2. Total EPR represented by colored transect (m/year) at Juan Gerónimo Ranch. Blue poligons indicate erosion (JGS) and progradation (JGN) areas. The location where the cliff retrogression is being surveyed (control point) is indicated with a white star (Bacino et al., 2019). (For interpretation of the references to color in this figure legend, the reader is referred to the Web version of this article.)

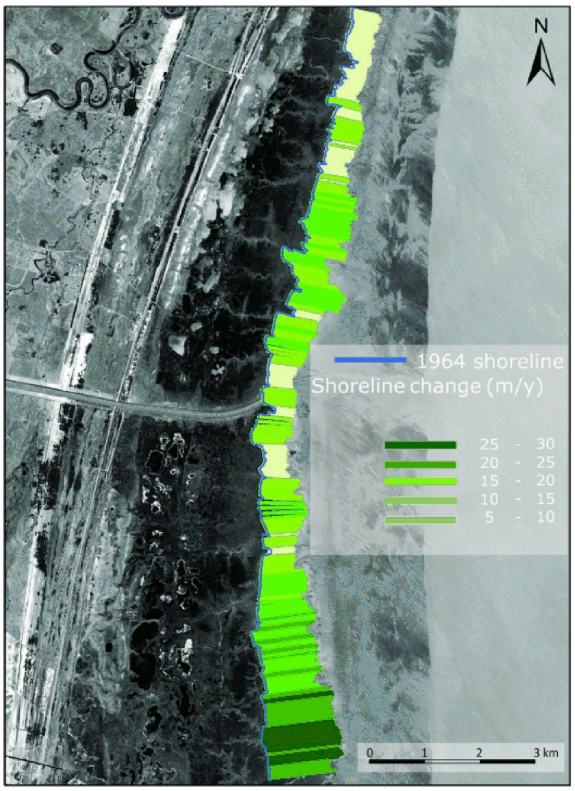

Fig. 3. Total EPR represented by colored transect (m/year) at Channel 18.

4.1.4. Channel 18

Channel 18, located in the middle of the bay (Fig. 3), presents total *NSM* and *EPR* equal to +734 m and +14.4 ± 0.1 m/year (accretion), respectively (period: 1964–2017). Recent *EPR* was estimated at +29.7 ± 0.1 m/year and the *NSM* at 230 m (period: 2010–2017).

4.1.5. Channel 1

The analysis of the coastal evolution at Channel 1 allows us to clearly distinguish two different zones (Fig. S2). At the northern sector (C1N), the total *EPR* was estimated at +3.3 ± 0.1 m/year (accretion) and, at the southern sector (C1S) the rate was estimated at −0.7 ± 0.1 m/year (erosion), between 1964 and 2017. At C1N the recent *EPR* was estimated at +3.5 ± 0.2 m/year (erosion) and at C1S at −0.3 ± 0.2 m/year (erosion), between 2003 and 2017. Based on measurements of the marsh edge position the annual total retreat rate (2010–2017) was estimated at −0.66 m/year at the northern C1S, near the boundary with C1N (Bacino et al., 2019).*EPR* computed for the closest transect to the control point (100 m far) was −2.3 ± 0.2 m/year (2003–2017).

4.1.6. Ajó River

Total *EPR* and *NSM* equal to −2.3 ± 0.1 m/year and −124 m (erosion), respectively, were estimated at Ajó River coastal area between 1964 and 2017 (Fig. 4). *EPR* and *NSM* of −5.6 ± 0.4 m/year and −46 m were estimated between 2009 and 2017. This is one of the most vulnerable areas of the bay due to its very low elevation with respect to the mean sea level (Tosi et al., 2013).

Estimated values of total and recent *EPR*, U_{EPR} and *NSM* are summarized in Table S1. Negative values correspond to shoreline retreat (erosion) and positive values to shoreline advance (progradation or accretion). For the total period (around 50 years), intense erosive conditions were detected at JGS (−4.2 m/year), Punta Indio (−3.8 m/year) and Ajó River (−2.3 m/year), and moderate erosion at C1S (−0.7 m/year) and Punta Piedras (−0.8 m/year). On the contrary, very intense accretion was identified at Channel 18 (+14.4 m/year), and lower values at C1N (+3.3 m/year) and JGN (+0.8 m/year). For the recent period the most intense erosion can be appreciated at JGS (−11.6 m/year), Punta Indio (−3.5 m/year) and Ajó River (−5.6 m/year), and moderate conditions at Punta Piedras (−2.0 m/year), JGN (−0.7 m/year) and C1S (−0.3 m/year). On the contrary, maximum accretion was identified at Channel 18 (+29.7 m/year) and lower values at C1N (+3.5 m/year). From the comparison of the total and recent *EPR* it can be concluded that, in general, the locations maintained (Punta Indio, C1N and C1S) or increased (Punta Piedras, JGS, Channel 18, and Ajó River) the erosion or accretion rates. The only exception is JGN. In this location, the total rate indicates that the shoreline was affected by a very low accretion (+0.8 m/year), but the recent rate corresponds to an area under slight erosive processes (−0.7 m/year).

EPR values (total period) in Samborombón Bay are schematically illustrated for the analyzed coastal areas (Fig. 5). Clear erosion can be

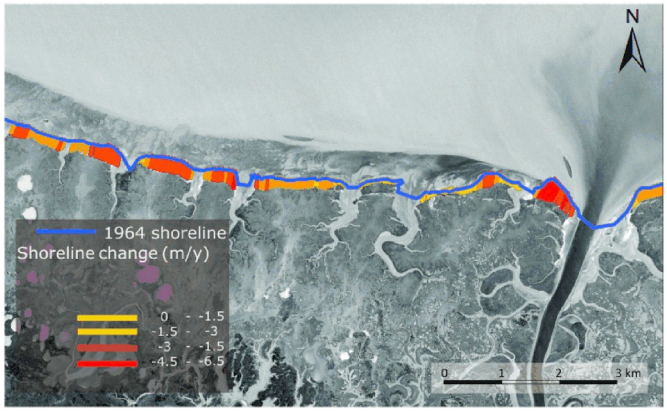

Fig. 4. Total EPR represented by colored transect (m/year) at Ajó River. where the cliff retrogression is being surveyed (control point) is indicated with a white star (Bacino et al., 2019).

appreciated at Punta Indio with the exceptions of two sites, located at 0.5 and 1.0 km, approximately, which are highly stable and present practically no erosion. The stability of these sites is probably due to the presence of relatively more consolidated materials on the coast. Southward, at Punta Piedras, there is a significant decrease in erosion, and the shoreline is practically stable at JGN. On the contrary, erosion begins to be very noticeable at JGS, from 6 km towards the southwest. At the center of the bay (Channel 18) accretion is very noticeable mainly from 5 km to the south of the channel mouth. The coastal area between the 4 and 6 km (Channel 1) seems to be a transitional zone between areas of weak accretion and erosion and, finally, clear erosion can be appreciated again at Ajó River. Summarizing, the results corresponding to the recent period indicate accretion at Channel 18 and C1N, and erosion over the rest of the bay.

4.2. Wave energy fluxes

Annual mean *Pi* (period: 1971–2018) was computed along the shoreline (Fig. 6.a). Highest values were estimated close Ajó River (124 J/ms) and Channel 1 (121 J/ms), at the southern sector of the bay, and near Juan Gerónimo Ranch (112 J/ms). Relatively lower *Pi* values were simulated at the center of the bay (around 90 J/ms) and at the north of Punta Piedras (lower than 60 J/ms). Annual mean Pl_N (period: 1971–2018) was also simulated along the shoreline of the bay. Pl_N flows predominantly southwards, from Punta Piedras to Channel 1, and flows westwards at Ajó River coastal area (Fig. 6.b). Maximum southward Pl_N can be observed near Juan Gerónimo Ranch (9.1 J/ms) and northeastward Channel 18(13.1 J/ms). Pl_N significantly decreases between Channel 18 and Channel 1 (<4 J/ms). Westward Pl_N was estimated at the southern sector of the bay (Ajó River) with the highest value in the bay (28.4 J/ms).

Simulated data series of annual mean Pl_N and *Pi* were analyzed at two adjacent sites (Juan Gerónimo Ranch and Salado River) in order to illustrate their temporal and spatial variabilities (Fig. 7). Pl_N presents practically the same variability at both locations and, in general, it is a little larger at Salado River than at Juan Gerónimo Ranch. These differences in the annual mean Pl_N could produce a slight divergence in the alongshore energy flux which would be associated with mild coastal erosion. Some exceptions can be appreciated in 1983, 1985, 1994, 1998, 2005 and 2018. Normal (southward) annual mean Pl_N were estimated at Salado River in these years, while atypical (northward) values were computed at Juan Gerónimo Ranch. The inversion in the annual mean Pl_N could produce light coastal erosion. There is only one year (1993) in which simulated Pl_N has inverse directions in both locations. In this year Pl_N at Juan Gerónimo Ranch is larger than at Salado River, which is associated with a possible accretion period. Data series of annual mean *Pi* presents a very similar variability at both adjacent locations (Fig. 7).

Relatively low variability is observed between 1971 and 1989. Mean *Pi* is around 22% greater at Juan Gerónimo Ranch than at Salado River. Mean *Pi* and its variability considerably increase from 1990 at both locations. Maximum *Pi* occurred at Salado River and Juan Gerónimo Ranch in 1993 and 2001 reaching values around 120 and 160 J/ms, respectively. In addition, Pl_N and *Pi* trends were computed from the monthly data series along the shoreline of the bay, using the seasonal Mann Kendall trend technique (Hirsch et al., 1982).Pl_N trend, significantly different from zero, was only detected at Ajó River, with a decrease of -3.1 ± 2 J/ms per decade (i.e. an increase of Pl_N in the westward direction) (Fig. 8). On the contrary, *Pi* trends (significantly different from zero) were detected along almost the entire shoreline of the bay, with maximum values at JGN, Channel 15 and C1N (2–3 J/ms per decade) and lower values at Punta Indio and JGS (1–2 J/ms per decade).*Pi* trend (not significantly different from zero) was found at Ajó River.

5. Discussion

The study of the evolution of the shoreline based only on field data is practically impossible to carry out at Samborombón Bay due to problems of accessibility to the coast, especially in the center of the bay (for instance, Channel 18). However, the analysis of different kinds of historical and recent images allows us to estimate the changes that have taken place. Since reliable sets of images are not available for the whole shoreline of the bay, the present study had to be developed at only six specific areas, in which the sequences of images had appropriate time coverage.

Significant rates of shoreline changes (i.e. erosion or accretion) were found at Samborombón Bay, which are relatively large in comparison with rates obtained in other salt marshes in the world. For instance, erosion rates of −11.6 m/year (2010–2016) were found at JGS (Table S1, Fig. 2) and a marsh expansion of almost +30 m/year (2010–2017) was estimated near to JGS, at Channel 18 (Table S1, Fig. 3). For instance, in Chesapeake Bay, Wrayf et al. (1995) computed a

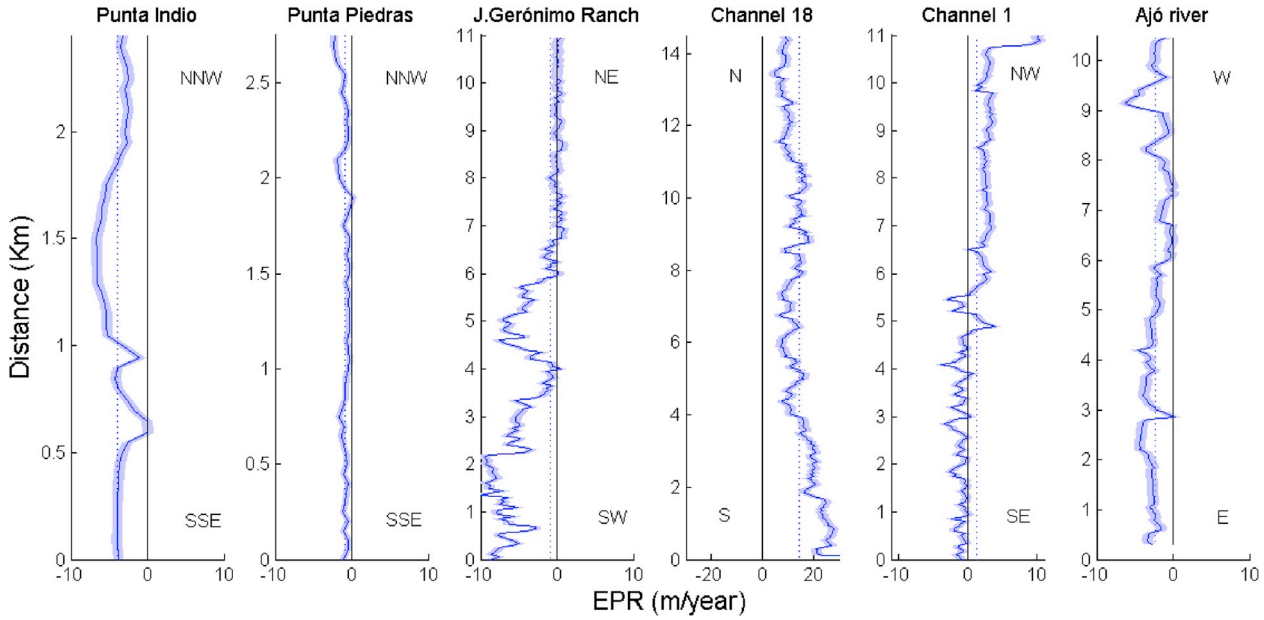

Fig. 5. EPR (m) along the shoreline (km) for the recient period. Mean EPR is indicated in dashed line.

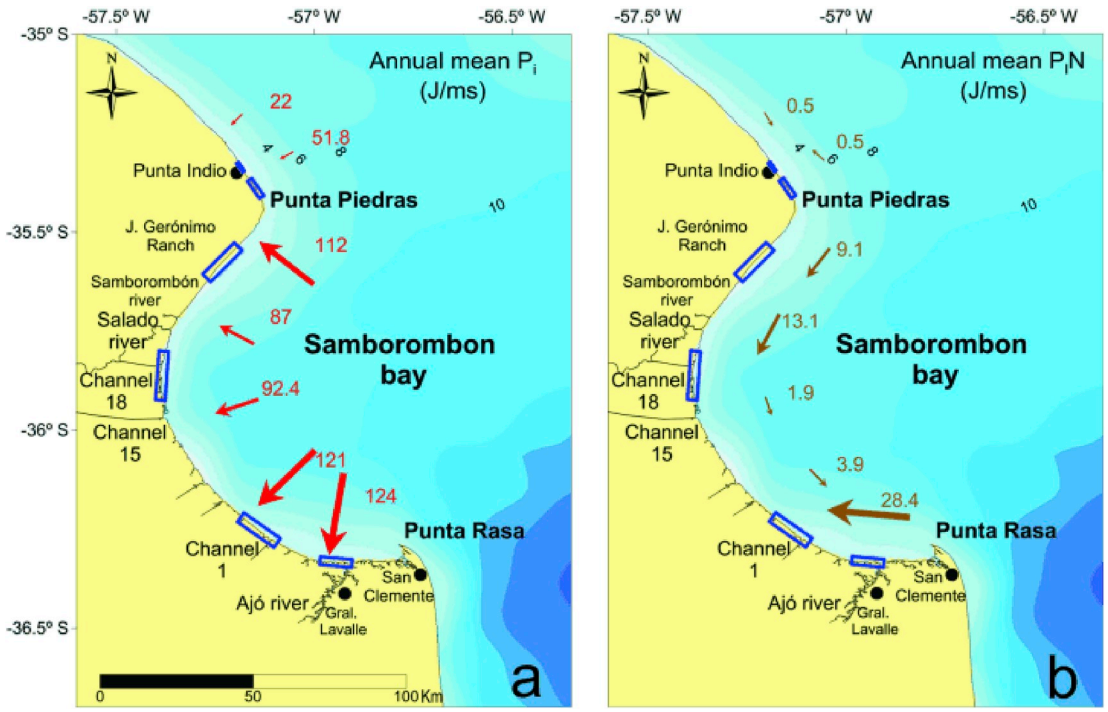

Fig. 6. (a) Annual mean Pi (red arrows, J/ms), and (b) annual mean Pl_N (brown arrows, J/ms). Bathymetric contours in meters. Analyzed coastal areas are pointed out in blue rectangles. (For interpretation of the references to color in this figure legend, the reader is referred to the Web version of this article.)

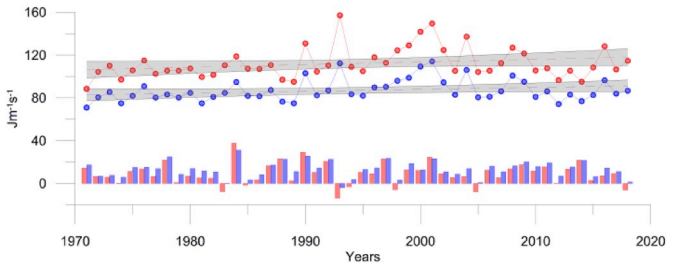

Fig. 7. Simulated data series of annual mean Pl_N (bars), and Pi (solid lines) at Juan Gerónimo Ranch (red) and Salado River (blue). Linear trends in Pi data series (dashed lines) and their uncertainties (grayish area) are also indicated. (For interpretation of the references to color in this figure legend, the reader is referred to the Web version of this article.)

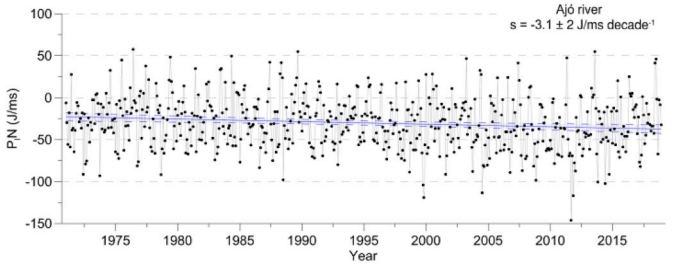

Fig. 8. Data series of Pl_N at Ajó River. Positive (negative) values of Pl_N indicate eastward (westward) fluxes. The calculated regression line (blue solid line) and its uncertainty (±95%, blue dashed line) are also shown. (For interpretation of the references to color in this figure legend, the reader is referred to the Web version of this article.)

long term erosion between 0.7 and 4.9 m/y and in the upper Delaware Bay a short term erosion rate was found between 0.2 and 7.3 m/y (Schwimmer, 2001). Long term shoreline changes studies in Chesapeake Bay and Venice Lagoon revealed that the wind-waves processes play a key role in sediment erosion and transport (Sanford and Gao, 2018; Tommasini et al., 2019). The accretion rate obtained is in agreement with the results obtained by Lamaro et al. (2009) and Tosi et al. (2013), who computed a marsh expansion of around +16 m/year (1968–1994) and +21 m/year (1972–2013), respectively, at the center of the bay. On the contrary, Lamaro et al. (2009) and Tosi et al. (2013) reported a stable shoreline at the southern and northern sectors of the bay. Differences between the results obtained in this work and those presented by Lamaro et al. (2009) and Tosi et al. (2013) are probably due to the lower resolution of the images used by these authors (Landsat 1,2,5 and 7, Spot 1 and SAC-C).The use of different techniques for inferring the shoreline change could also partially explain some differences in the rates estimated by different authors.

Based on image analysis, it was seen that during the last decade both extremes of the bay are being eroded and, in some areas (Channel 18 and C1N), the coast is being constructed. The annual shoreline movement was quantified through the computation of the *EPR* (m/year). In general, the computed *EPR* is higher in the recent period (the last decade, approximately) than in the total period (approximately the last 50 years) which reveals the acceleration of the coastal processes during the last years. Such acceleration of the erosive processes at Somborombón Bay was previously suggested by Codignotto et al. (2012).

It is widely known that swell can propagate into the Río de la Plata from the ocean (Dragani and Romero, 2004). However, swell is rather moderate and is not energetic enough to significantly influence the shoreline sediment budget along the bay. Wave spectra obtained with a directional buoy (Datawell Waverider Mark II, period: 1996–2001) were used to describe the swell in the Río de la Plata. It was obtained that swell heights are lower than the mean sea height in the Río de la Plata mouth. Swell is characterized by heights between 0.40 and 0.80 m, periods between 11 and 15 s, and propagation directions from the SE (60% of cases), SSE (20%), ESE (10%), E and S (less than 5% of cases). The frequency of occurrence of swell is maximum in winter, followed by the fall and the spring, and then the summer.

Higher *Pi* was found at the extremes of the bay and lower values at the center (around Channel 18). Positive *Pi* trends were detected along

almost the entire shoreline of the bay (except at Ajó River). Positive trends in *Pi* are also in agreement with the acceleration reported by Codignotto et al. (2012). On the other hand, Pl_N presents a convergent pattern in the coastal area of the bay. Lower Pl_N are also found at the center of the bay, between Channel 1 and Channel 18. Pl_N presents a significant trend only at Ajó River, therefore it can be concluded that the alongshore wave energy is quite stable in time along the bay. It should nevertheless be highlighted that in the single place where Pl_N trend is significantly different to zero (Ajó River) *Pi* does not present a significant trend. Consequently, while the capability of erosion (*Pi*) remains quite stable in time, the capability of transport (Pl_N) is increasing at Ajó River. The spatial variability in the annual mean Pl_N was particularly studied at two adjacent sites (Salado River and Juan Gerónimo Ranch). It was noted that slight differences in Pl_N can produce differential (low) coastal erosion, and inversions in Pl_N (i.e. differences in the sign of Pl_N between both sites) would produce more coastal erosion, at least during some months of a particular year (Fig. 7). Consequently, it is clear that *EPR* rates, estimated from the analysis of images corresponding to two particular instants, are very useful to provide annual mean rates. Nevertheless, the analysis of the Pl_N variability, not only in intensity but also in direction, allows investigation of the time evolution of the erosion and accretion processes along the coast.

Even though the hydro-sedimentary processes at the coastal area of Samborombón Bay are highly complex, an elementary conceptual model is proposed which aims to explain some basic mechanisms about the sediment balance in the system (i.e. the coastal area of the bay). A sketch of this conceptual model is presented in Fig. 9.

Based on the analysis of aerial photographs and high-resolution satellite images, *in situ* measurements of cliff retrogression, and numerical simulations of waves (SWAN model), the hydro-sedimentary processes at the coastal area of Samborombón Bay can be explained as follows:

(i) *Pi* is considered the dominant erosional agent of the coastal bay.
(ii) It was found erosion (red coast, Fig. 9) at the extremes of the bay (Fig. 10.a), and a marsh expansion (green coast, Fig. 9) at the center (Fig. 10.b).
(iii) The locations of higher *Pi* are in agreement with the main erosional areas (Fig. 6.a).
(iv) The eroded sediment (at bay extremes) is transported towards the center of the bay through a convergent pattern of Pl_N (Fig. 6.b, blue arrows in Fig. 9).
(v) The convergence zone of Pl_N (between blue arrows, Fig. 9) is in agreement with the accretion area (green coast, Fig. 9). New flora can be appreciated at the foot of the scarp, showing the capability of the system in building new low marsh (Fig. 10.b).
(vi) Sediments eroded from the coast of the bay (red coast, Fig. 9) and sediments coming from external sources (for example, Paraná River, pluvial channels, or re-suspended materials from the Río de la Plata bottom; brown arrow, Fig. 9) contribute to the vertical increase of the marsh (driven by mean sea level rise and storm surge events) and to the expansion seaward of low marshes at the center of the bay (Fig. 10.b).

Marshlands around the world have proved to be resilient to mean SLR in the vertical direction, accreting faster (Kirwan et al., 2016; Schuerch et al., 2016). Schuerch et al. (2016) inferred a vertical accretion rate of +2.6 cm/year near Salado River, which is one order of magnitude higher than the mean SLR estimated by D'Onofrio et al. (2008)for the Río de la Plata estuary (+0.17 cm/year). Based on age-dated cores analysis Schuerch et al. (2016) suggested the hypothesis that the vertical accretion of the marsh could be associated with sediments transported by the Río de la Plata rather than supplied by Salado River. This could be a sign of a healthy salt marsh in terms of constant vertical growth and import of sediments (Ganju et al., 2017). However, Hopkinson et al. (2018) found that to keep the vertical accretion rate above mean sea level at Plum Island Sound estuary (Massachusetts), it

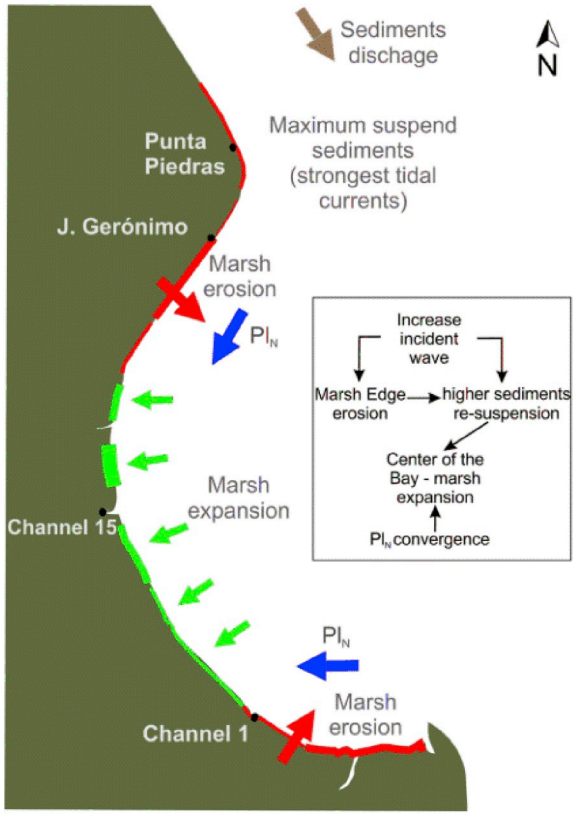

Fig. 9. Hydro-sedimentary processes at the coastal area of Samborombón Bay: a sketch of the proposed conceptual model. Red (green) arrow indicates sediment input (output) to (from) the coastal water. Red (green) coast indicates erosion (progradation). Blue arrow indicates the longshore energy flux direction. (For interpretation of the references to color in this figure legend, the reader is referred to the Web version of this article.)

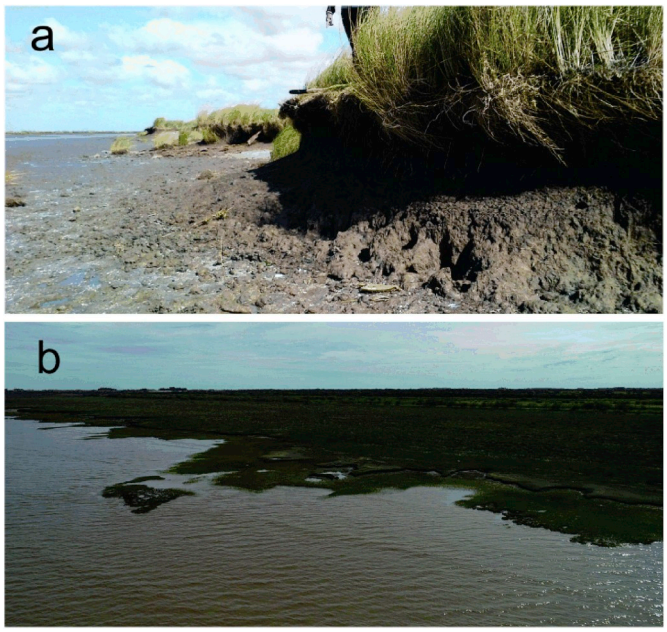

Fig. 10. (a) Eroded scarp at southern Channel 1, and (b) formation of the new marsh at the center of Samborombón Bay, taken from an unmanned aerial vehicle (UAV) at 40 m height.

would be essential that the sediment was provided from eroded marsh edges. Also, Hopkinson et al. (2018) found that tidal flats and bay bottoms could be an important source of sediments to maintain the balance of the system.

The decrease in the sediment supply has been highlighted in many estuaries around the world, playing a critical role in the sediment supply to the salt marsh systems, as in reducing the marsh area. For example, retreating salt-marshes in the Lagoon of Venice have been reported, where sediment inputs have been completely eliminated through Jetty construction at the Lagoon inlets (Day et al., 1998). In the 20th century, the Delaware Estuary and the Chesapeake Bay were characterized by a decrease of riverine sediment influx, which constitutes the main sediment source for marshes (Mariotti and Fagherazzi, 2013). Projections show that this sediment starvation may be exacerbated by increasing dam construction (Schuerch et al., 2018) and land-use change (Pelletier et al., 2015).

The annual amount of sediment that flows into to the Río de la Plata Estuary, mainly from the Paraná River, is around $160x10^6$ metric tons (Dogliotti et al., 2016). An important proportion of this sedimentary load is transported in suspension, principally along the southern coast of the Río de la Plata (Moreira et al., 2013; Fossati et al., 2014a), and a part of this is settled on the bottom, but it can be resuspended. Two main mechanisms are able to resuspend the bottom sediment: strong tidal currents, for instance, at Punta Piedras coastal area (Simionato et al., 2004), and intense wind waves during storms (Fossati et al., 2014b). In addition, a relatively lower amount of sediments could be entering the Río de la Plata due to the widening of the tidal channels networks produced by the SLR (Kirwan and Megonigal, 2013; Watson et al., 2017). Consequently, external sources of sediments (for example, Paraná River, tidal channels, or bottom resuspended materials) have to be considered to complete this simplified conceptual model. These sediments could enter the bay coastal area, be transported to the center of the bay by longshore currents, or contribute to the vertical increase of the marsh during storm surge events.

Finally, the boundary between the areas of retreatment (bay extremes) and accretion (bay center), are zones of transition, which could shift from being predominantly erosive to constructive areas. Then, the analysis of the shoreline evolution would become more complex in these zones. As a case in point, the long term retreatment at JGS, where the mean erosion rates almost triplicate from 1964 to 2010 to 2010–2016 (Table S1), could be the result of positive feedback. The amount of sediments arriving from NE would be lower than the sediment delivered from SSW (comparing the Pl), resulting in a continuous sediment deficit (Fig. 6). The removed marsh edge and mudflat sediments could remain available for coastal salt marshes to grow vertically or for longshore transport. In both cases, the tidal flat is exporting sediments and leading the system out of equilibrium. This sediment redistribution was observed in the UK east coast (Schuerch et al., 2019), describing the close coupling of the sediment dynamics on the tidal mudflat with those on the marsh surface. These authors explained the vertical marsh growth via the majority of the sediment being removed from marsh edge and mudflat, leading to an instability that could be indicating a system adaptation to a new equilibrium, reducing salt marsh area. The export of sediments from JGS favors the adjacent coastal sector at the central bay, where long term annual mean wave energy flux decreases by ~25% for incident waves (Fig. 6). The flux pattern and a significant reduction in the wave energy, generate an availability of sediments at this sector, allowing pioneer vegetation to colonize tidal flats supporting the bed accretion and expansion seaward, even in the presence of waves (Wang et al., 2017). Rapidly accumulating mudflats provide an ideal condition for S. *alterniflora* expansion, as observed in the Yangtze Estuary, China (Xiao et al., 2010). The horizontal marsh growth - through the establishment of pioneer species - can occur by means of two different mechanisms: seeds disperse, deposit and germinate in the presence of windows of opportunity (lack of environmental stressors, by inundation, currents, waves and storm surges) and lateral clonal propagation of the marsh edge, this is the lateral below-ground expansion of rhizomes and growth of new above-ground shoots, beneficiating from clonal integration and surviving critical conditions (Silinski et al., 2016). This positive feedback between vegetation and sediments could only occur if the sediments were arriving at the marsh boundary or were provided as a product of the erosion (Hopkinson et al., 2018). van der Wal and Pye (2004) observed that the marsh edge retreated more slowly when pioneer flora begins to settle at the foot of the scarp because the vegetation helps to increase the mudflat elevation, and enhance the dissipation of wave and tidal energy.

6. Conclusions

The aim of this work was to quantify the shoreline change rates at six control areas disposed along Samborombón Bay, Río de la Plata. Digital Shore Analysis System 4.3 (DSAS) was used to process aerial photographs and high-resolution satellite images (Spot7/Quickbird/WorldView2/Pleiades) of the coast of the bay. Two periods were considered in this study: a total period (last 50 years) and a recent period (last decade, approximately). Intense erosive conditions (around −3 m/year) were detected at JGS, Punta Indio and Ajó River, and moderate (around −1 m/year) erosion was detected at C1S and Punta Piedras in the total period. On the contrary, significant accretion was identified at Channel 18 (+14.4 m/year) and lower values (around +1 or +2 m/year) were observed at C1N and JGN. For the recent period the most intense erosion was appreciated at JGS (−11.6 m/year), lower values (around −4 or −6 m/year) were detected at Punta Indio and Ajó River, and moderate values (lower than −2 m/year) were observed at C1S, Punta Piedras and JGN. Maximum accretion was identified at Channel 18 (+29.7 m/year). From the comparison of the results obtained between both periods (total and recent), it is concluded that Punta Piedras, JGS, Channel 18, C1N, C1S, and Ajó River have increased their erosion and accretion rates during the last years. This would be in agreement with a possible acceleration in the erosive processes which was suggested by Codignotto et al. (2012). The only exception would be JGN, where the coastal processes seem to have changed from accretion to erosion. In this location, the total rate indicated that the shoreline was under a very low accretion (+0.8 m/year), but the recent rate shows slight erosive processes (−0.7 m/year).

Pl_N and *Pi* were computed from wave parameters simulated with SWAN model (period: 1979–2018). Highest annual mean *Pi* values were estimated close Ajó River and Channel 1, at the southern sector of the bay, and near Juan Gerónimo Ranch (112 J/ms), at the northern sector of the bay. On the contrary, lower values of annual mean *Pi* were obtained at the center of the bay. It was also found that annual mean Pl_N flows predominantly southwards, from Punta Piedras to Channel 1, and westwards at Ajó River coastal area (Fig. 6.b). Consequently, Pl_N would be showing a convergent pattern in the coastal area of the bay. In addition, some differences in the annual mean Pl_N between two adjacent locations were detected. These differences would produce a slight divergence in Pl_N which would be associated with mild coastal erosion. Annual mean *Pi* shows relatively low variability between 1971 and 1989, and the values considerably increase from 1990 to the present. Positive trends were found in *Pi* data series for almost all the coast of the bay. On the contrary, Pl_N only presents a significant trend at Ajó River, at the southern end of the bay. Then, it can be concluded that while the capability of erosion (*Pi*) is increasing, the capacity of transport (Pl_N) is quite stable along almost the entire coastline of the bay.

Finally, based on the analysis of different images, systematic measurements of the cliff retrogression and numerical simulations of waves carried out with SWAN model, the hydro-sedimentary processes at the coastal area of Samborombón Bay were interpreted, and a simple conceptual model (Fig. 8) which includes internal and external sources of sediments is proposed.

CRediT authorship contribution statement

Guido L. Bacino: Conceptualization, Methodology, Writing - original draft. **Walter C. Dragani:** Conceptualization, Writing - original draft, Project administration, Funding acquisition. **Jorge O. Codignotto:** Conceptualization. **Andrés E. Pescio:** Methodology, Formal analysis. **Marcelo O. Farenga:** Validation.

Acknowledgements

This study was parcially financially supported by the PIP 112-201501-00174 (CONICET: Consejo Nacional de Investigaciones Científicas y Técnicas de Argentina) grant. We wish to thank a lot to both anonymous reviewers and the editor for their comments and suggestions. We are particularly grateful with José Bedmar (SEGEMAR) for his valuable suggestions in the revision of this manuscript and with Daniel Abriola (CNEA) for helping in the English revision.

Appendix A. Supplementary data

Supplementary data to this article can be found online at https://doi.org/10.1016/j.ecss.2020.106659.

References

Aiello, A., Canora, F., Pasquariello, G., Spilotro, G., 2013. Shoreline variations and coastal dynamics: a space e time data analysis of the Jonian littoral. Italy. Estuar. Coast. Shelf Sci. 129, 124–135. https://doi.org/10.1016/j.ecss.2013.06.012.

Anisfeld, S.C., Cooper, K.R., Kemp, A.C., 2017. Upslope development of a tidal marsh as a function of upland land use. Global Change Biol. 23, 755–766. https://doi.org/10.1111/gcb.13398.

Anthony, E.J., Brunier, G., Besset, M., Goichot, M., 2015. Linking rapid erosion of the Mekong River delta to human activities. Sci. Rep. 5, 14745. https://doi.org/10.1038/srep14745.

Bacino, G.L., Dragani, W.C., Codignotto, J.O., 2019. Changes in wave climate and its impact on the coastal erosion in Samborombón Bay , Río de la Plata estuary , Argentina. Estuar. Coast Shelf Sci. 219, 71–80. https://doi.org/10.1016/j.ecss.2019.01.011.

Bendoni, M., Mel, R., Solari, L., Lanzoni, S., Francalanci, S., Oumeraci, H., 2016. Insights into lateral marsh retreat mechanism through localized field measurements. Water Resour. Res. 52, 1446–1464. https://doi.org/10.1002/2015WR018249.

Booij, N., Ris, R.C., Holthuijsen, L.H., 1999. A third-generation wave model for coastal regions. Part 1. Model description and validation. J. Geophys. Res. 104 (C4), 7649–7666. https://doi.org/10.1029/98JC02622.

Carol, E.S., Braga, F., Kruse, E.E., Tosi, L., 2014. A retrospective assessment of the hydrological conditions of the Samborombón coastland (Argentina). Ecol. Eng. 67, 223–237. https://doi.org/10.1016/j.ecoleng.2014.03.081.

Cellone, F., Carol, E., Tosi, L., 2016. Coastal erosion and loss of wetlands in the middle Río de la Plata estuary (Argentina). Appl. Geogr. 76, 37–48. https://doi.org/10.1016/j.apgeog.2016.09.014.

CERC, 1984. Shore Protection Manual. U.S. Army Corps of Engineers, Coastal Engineering Research Center. U.S. Government Printing Office, Washington. D.C., p. 640

Codignotto, J.O., Dragani, W.C., Martin, P.B., Simionato, C.G., Medina, R.a., Alonso, G., 2012. Wind-wave climate change and increasing erosion in the outer Río de la Plata, Argentina. Continent. Shelf Res. 38, 110–116. https://doi.org/10.1016/j.csr.2012.03.013.

Couvillion, B.R., Beck, H., Schoolmaster, D., Fischer, M., 2017. Land area change in coastal Louisiana (1932 to 2016). U.S. Geol. Surv. Sci. Investig. Map 3381, 16.

Cowart, L., Walsh, J.P., Corbett, D.R., 2010. Analyzing estuarine shoreline change: a case study of cedar island, North Carolina. J. Coast Res. 26, 817–830. https://doi.org/10.2112/JCOASTRES-D-09-00117.1.

Currin, C., Davis, J., Baron, L.C., Malhotra, A., Fonseca, M., 2015. Shoreline change in the New River estuary, North Carolina: rates and consequences. J. Coast Res. 51 (5), 1069–1077. https://doi.org/10.2112/JCOASTRES-D-14-00127.1.

Day, J.W., Scarton, F., Rismondo, A., Are, D., 1998. Rapid deterioration of a salt marsh in Venice Lagoon, Italy. J. Coast Res. 14, 583–590.

Dean, R.G., Dalrymple, R.A., 2001. Coastal Processes with Engineering Applications. Cambridge University Press, Cambridge. https://doi.org/10.1017/CBO9780511754500.

Dogliotti, A.I., Ruddick, K., Guerrero, R., 2016. Seasonal and inter-annual turbidity variability in the Río de la Plata from 15 years of MODIS: el Niño dilution effect Estuarine. Estuar. Coast Shelf Sci. 182, 27–39. https://doi.org/10.1016/j.ecss.2016.09.013.

D'Onofrio, E.E., Fiore, M.M.E., Pousa, J.L., 2008. Changes in the regime of storm surges at Buenos Aires, Argentina. J. Coast Res. 24, 260–265. https://doi.org/10.2112/05-0588.1.

D'Onofrio, E.E., Oreiro, F., Fiore, M.M.E., 2012. Simplified empirical astronomical tide model — an application for the Río de la Plata estuary. Comput. Geosci. 44, 196–202. https://doi.org/10.1016/j.cageo.2011.09.019.

Dragani, W.C., Garavento, E., Simionato, C.G., Nuñez, M.N., Martin, P., Campos, M.I., 2008. Wave simulation in the outer Río de la Plata estuary: evaluation of SWAN model. J. Waterw. Port, Coast. Ocean Eng. 134, 299–305. https://doi.org/10.1061/(ASCE)0733-950X(2008)134:5(299).

Dragani, W.C., Martin, P.B., Simionato, C.G., Campos, M.I., 2010. Are wind wave heights increasing in south-eastern south American continental shelf between 32°S and 40°S? Continent. Shelf Res. 30, 481–490. https://doi.org/10.1016/j.csr.2010.01.002.

Dragani, W.C., Romero, S.I., 2004. Impact of a possible local wind change on the wave climate in the upper Río de la Plata. Int. J. Climatol. 24 (9), 1149–1157. https://doi.org/10.1002/joc.1049.

Elsey-Quirk, T., Mariotti, G., Valentine, K., Raper, K., 2019. Retreating marsh shoreline creates hotspots of high-marsh plant diversity. Sci. Rep. 9, 1–9. https://doi.org/10.1038/s41598-019-42119-8.

Fagherazzi, S., Mariotti, G., Wiberg, P.L., 2013. Marsh collapse does not require sea level rise. Oceanography 26, 70–77. https://doi.org/10.5670/oceanog.2013.47.

FitzGerald, D.M., Hughes, Z., 2019. Marsh processes and their response to climate change and sea-level rise. Annu. Rev. Earth Planet Sci. 47, 481–517. https://doi.org/10.1146/annurev-earth-082517-010255.

Fletcher, C.H., Richmond, B., Rooney, J., Barbee, M., Lim, S.C., 2003. Mapping shoreline change using digital orthophotogrammetry on maui, Hawaii. J. Coast. Res. SPEC. ISS. 38, 106–124.

Fletcher, C.H., Romine, B., Genz, A.S., Barbee, M., Dyer, M., Anderson, T., Lim, S.C., Vitousek, S., Bochicchio, C., Richmond, B., 2011. National Assessment of Shoreline Change: Historical Shoreline Change in the Hawaiian Islands. U.S. Geological Survey Open-File Report.

Fossati, M., Cayocca, F., Piedra-CuevaI, I., 2014a. Fine sediment dynamics in the Río de la Plata. Adv. Geosci. 39, 75–80. https://doi.org/10.5194/adgeo-39-75-2014.

Fossati, M., Santoro, P., Mosquera, R., Martínez, C., Ghiardo, F., Ezzatti, P., Pedocchi, F., Piedra-CuevaI, I., 2014b. Dinámica de flujo, del campo salino y de los sedimentos finos en el Río de la Plata. RIBAGUA - Rev. Iberoam. del Agua 1, 48–63. https://doi.org/10.1016/S2386-3781(15)30007-4.

Ganju, N.K., Defne, Z., Kirwan, M.L., Fagherazzi, S., D'Alpaos, A., Carniello, L., 2017. Spatially integrative metrics reveal hidden vulnerability of microtidal salt marshes. Nat. Commun. 8, 14156. https://doi.org/10.1038/ncomms14156.

GEBCO, 2003. User guide to the centenary edition of the GEBCO Digital Atlas and its data sets. In: Jones, M.T. (Ed.), Natural Environment Research Council. Natural Environment Research Council.

Genz, A.S., Fletcher, C.H., Dunn, R.a., Frazer, L.N., Rooney, J.J., 2007. The predictive accuracy of shoreline change rate methods and alongshore beach variation on maui, Hawaii. J. Coast Res. 231, 87–105. https://doi.org/10.2112/05-0521.1.

Himmelstoss, E.A., 2009. DSAS 4.0 installation instructions and user guide.U.S. Geological survey open-file report 2008-1278. *updated for version 4.3.. In: Thieler, E.R., Himmelstoss, E.A., Zichichi, J.L., Ergul, A. (Eds.), Digital Shoreline Analysis System (DSAS) Version 4.0 — an ArcGIS Extension for Calculating Shoreline Change, p. 79.

Hirsch, R.M., Slack, J.R., Smith, R.A., 1982. Techniques of trend analysis for monthly water quality data. Water Resour. Res. 18, 107–121.

Hopkinson, C.S., Morris, J.T., Fagherazzi, S., Wollheim, W.M., Raymond, P.A., 2018. Lateral marsh edge erosion as a source of sediments for vertical marsh accretion. J. Geophys. Res. Biogeosciences 123, 2444–2465. https://doi.org/10.1029/2017JG004358.

Hughes, M.L., McDowell, P.F., Marcus, W.A., 2006. Accuracy assessment of georectified aerial photographs: implications for measuring lateral channel movement in a GIS. Geomorphology 74, 1–16. https://doi.org/10.1016/j.geomorph.2005.07.001.

Isacch, J.P., Costa, C.S.B., Rodríguez-Gallego, L., Conde, D., Escapa, M., Gagliardini, D. A., Iribarne, O.O., 2006. Distribution of saltmarsh plant communities associated with environmental factors along a latitudinal gradient on the south-west Atlantic coast. J. Biogeogr. 33, 888–900. https://doi.org/10.1111/j.1365-2699.2006.01461.x.

Kirwan, M.L., Megonigal, J.P., 2013. Tidal wetland stability in the face of human impacts and sea-level rise. Nature 504, 53–60. https://doi.org/10.1038/nature12856.

Kirwan, M.L., Temmerman, S., Skeehan, E.E., Guntenspergen, G.R., Fagherazzi, S., 2016. Overestimation of marsh vulnerability to sea level rise. Nat. Clim. Change 6, 253–260. https://doi.org/10.1038/nclimate2909.

Lamaro, A. a, Torrusio, S.E., Ulibarrena, J., Mugni, H., Bonetto, C., 2009. Mapping of coastal changes applying maps , satellite images and GIS in Samborombón bay, Argentina. Int. J. Ecol. Dev. 12, 15–27.

Leonardi, N., Defne, Z., Ganju, N.K., Fagherazzi, S., 2016. Salt marsh erosion rates and boundary features in a shallow Bay. J. Geophys. Res. Earth Surf. 121, 1861–1875. https://doi.org/10.1002/2016JF003975.

Marani, M., D'Alpaos, A., Lanzoni, S., Santalucia, M., 2011. Understanding and predicting wave erosion of marsh edges. Geophys. Res. Lett. 38, 1–5. https://doi.org/10.1029/2011GL048995.

Mariotti, G., Fagherazzi, S., 2013. Critical width of tidal flats triggers marsh collapse in the absence of sea-level rise. Proc. Natl. Acad. Sci. U.S.A. 110, 5353–5356. https://doi.org/10.1073/pnas.1219600110.

Martin, P., Dragani, W., Cerne, B., Alonso, G., Pescio, A., Prario, B., 2012. Numerical simulation of wind waves on the Río de la Plata: evaluation of four global atmospheric databases. Braz. J. Oceanogr. 60, 501–511. https://doi.org/10.1590/S1679-87592012000400008.

Mentaschi, L., Vousdoukas, M.I., Pekel, J.F., Voukouvalas, E., Feyen, L., 2018. Global long-term observations of coastal erosion and accretion. Sci. Rep. 8, 1–11. https://doi.org/10.1038/s41598-018-30904-w.

Moreira, D., Simionato, C.G., Gohin, F., Cayocca, F., Luz Clara Tejedor, M., 2013. Suspended matter mean distribution and seasonal cycle in the Río de La Plata estuary and the adjacent shelf from ocean color satellite (MODIS) and in-situ observations. Continent. Shelf Res. 68, 51–66. https://doi.org/10.1016/j.csr.2013.08.015.

Pelletier, J.D., Murray, a B., Pierce, J.L., Bierman, P.R., Breshears, D.D., Crosby, B.T., Ellis, M., Foufoula-georgiou, E., Heimsath, A.M., Houser, C., Lancaster, N., Marani, M., Merritts, D.J., Moore, L.J., Pederson, J.L., Poulos, M.J., Rittenour, T.M., Rowland, J.C., Ruggiero, P., Ward, D.J., Wickert, A.D., Yager, E.M., 2015. Forecasting the response of Earth 's surface to future climatic and land use changes: a review of methods and research needs. Earth Futur 3, 220–251. https://doi.org/10.1002/2014EF000290.

Piola, A.R., García, O.A., 1993. Publicación H-670. Atlas oceanográfico de la cuenca Argentina Occidental y de la plataforma continental lindera. Servicio de Hidrografía Naval, Armada Argentina, p. 267 (Ciudad de Buenos Aires).

Pratolongo, P., Mazzon, C., Zapperi, G., Piovan, M.J., Brinson, M., 2013. Land cover changes in tidal salt marshes of the Bahía Blanca estuary (Argentina) during the past 40 years. Estuar. Coast Shelf Sci. 133, 23–31. https://doi.org/10.1016/j.ecss.2013.07.016.

Priestas, A., Mariotti, G., Leonardi, N., Fagherazzi, S., 2015. Coupled wave energy and erosion dynamics along a salt marsh boundary, hog island bay, Virginia, USA. J. Mar. Sci. Eng. 3, 1041–1065. https://doi.org/10.3390/jmse3031041.

Raabe, E.A., Stumpf, R.P., 2015. Expansion of tidal marsh in response to sea-level rise: gulf coast of Florida, USA. Estuar. Coast 39, 145–157. https://doi.org/10.1007/s12237-015-9974-y.

Sanford, L.P., Gao, J., 2018. Influences of wave climate and sea level on shoreline erosion rates in the Maryland Chesapeake bay. Estuar. Coast 41, 19–37. https://doi.org/10.1007/s12237-017-0257-7.

Schieder, N.W., Walters, D.C., Kirwan, M.L., 2017. Massive upland to wetland conversion compensated for historical marsh loss in Chesapeake bay, USA. Estuar. Coast 41, 940–951. https://doi.org/10.1007/s12237-017-0336-9 Massive.

Schnack, E.J., 2010. Determinación de la línea de ribera desde la bahía Samborombón hasta Necochea.

Schuerch, M., Scholten, J., Carretero, S., García-Rodríguez, F., Kumbier, K., Baechtiger, M., Liebetrau, V., 2016. The effect of long-term and decadal climate and hydrology variations on estuarine marsh dynamics: an identifying case study from the Río de la Plata. Geomorphology 269, 122–132. https://doi.org/10.1016/j.geomorph.2016.06.029.

Schuerch, M., Spencer, T., Evans, B., 2019. Coupling between tidal mudflats and salt marshes affects marsh morphology. Mar. Geol. 412, 95–106. https://doi.org/10.1016/j.margeo.2019.03.008.

Schuerch, M., Spencer, T., Temmerman, S., Kirwan, M.L., Wolff, C., Lincke, D., McOwen, C.J., Pickering, M.D., Reef, R., Vafeidis, A.T., Hinkel, J., Nicholls, R.J., Brown, S., 2018. Future response of global coastal wetlands to sea-level rise. Nature 561, 231–234. https://doi.org/10.1038/s41586-018-0476-5.

Schwimmer, R., 2001. Rates and processes of marsh shoreline erosion in Rehoboth Bay, Delaware, USA. J. Coast Res. 17, 672–683. https://doi.org/10.2307/4300218.

SHN, 1986. Mar argentino, de Río de la Plata al Cabo de Hornos In: Carta Náutica, fourth ed., vol. 50. Servicio de Hidrografia Naval, Armada Argentina.

SHN, 1992. Acceso al Río de la Plata, Carta Náutica H1, fifth ed. Servicio de Hidrografia Naval, Armada Argentina.

SHN, 1999. Río de la Plata Exterior, Carta Náutica H113, second ed. Servicio de Hidrografia Naval, Armada Argentina.

SHN, 1999. Río de la Plata Medio y Superior, Carta Náutica H116, fourth ed. Servicio de Hidrografia Naval, Armada Argentina.

Silinski, A., Fransen, E., Bouma, T.J., Meire, P., Temmerman, S., 2016. Unravelling the controls of lateral expansion and elevation change of pioneer tidal marshes. Geomorphology 274, 106–115. https://doi.org/10.1016/j.geomorph.2016.09.006.

Simionato, C.G., Dragani, W., Nuñez, M., Engel, M., 2004. A set of 3-D nested models for tidal propagation from the argentinean continental shelf to the Río de la Plata estuary - Part II. M2. J. Coast. Res. 20, 903–912.

Simionato, C.G., Meccia, V.L., Dragani, W.C., Nuñez, M.N., 2006. On the use of the NCEP/NCAR surface winds for modeling barotropic circulation in the Río de la Plata Estuary. Estuar. Coast Shelf Sci. 70, 195–206. https://doi.org/10.1016/j.ecss.2006.05.047.

Simionato, C.G., Meccia, V.L., Guerrero, R.A., Dragani, W.C., Nuñez, M.N., 2007. The Río de la Plata estuary response to wind variability in synoptic to intra-seasonal scales: 2. Currents' vertical structure and its implications for the salt wedge structure. J. Geophys. Res. 112, C07005. https://doi.org/10.1029/2006JC003815.

Simionato, C.G., Vera, C.S., Siegismund, F., 2005. Surface wind variability on seasonal and interannual scales over Río de la Plata area. J. Coast Res. 214, 770–783. https://doi.org/10.2112/008-NIS.1.

Thieler, E.R., Danforth, W.W., Danfortht, W.W., 1994. Historical shoreline mapping (I): improving techniques and reducing positioning errors. J. Coast Res. 10, 549–563.

Thieler, E.R., Himmelstoss, E.A., Zichichi, J.L., Ergul, A., 2009. Digital Shoreline Analysis System (DSAS) Version 4.0— an ArcGIS Extension for Calculating Shoreline Change: U.S. Geological Survey Open-File Report 2008-1278.

Tommasini, L., Carniello, L., Ghinassi, M., Roner, M., D'Alpaos, A., 2019. Changes in the wind-wave field and related salt-marsh lateral erosion: inferences from the evolution of the Venice Lagoon in the last four centuries. Earth Surf. Process. Landforms 44, 1633–1646. https://doi.org/10.1002/esp.4599.

Tosi, L., Kruse, E.E., Braga, F., Carol, E.S., Carretero, S.C., Pousa, J.L., Rizzetto, F., Teatini, P., 2013. Hydro-morphologic setting of the Samborombón Bay (Argentina) at the end of the 21st century. Nat. Hazards Earth Syst. Sci. 13, 523–534. https://doi.org/10.5194/nhess-13-523-2013.

van der Wal, D., Pye, K., 2004. Patterns, rates and possible causes of saltmarsh erosion in the Greater Thames area (UK). Geomorphology 61, 373–391. https://doi.org/10.1016/j.geomorph.2004.02.005.

Violante, R.A., Cavallotto, J.L., 2004. Evolution of the semi-enclosed basins and surrounding coastal plains adjacent to the Pampean region. Argentina. Polish Geol. Inst. Spec. Pap. 11, 59–70.

Wang, H., van der Wal, D., Li, X., Belzen, J. van, Herman, P.M.J., Hu, Z., Ge, Z., Zhang, L., Bouma, T.J., 2017. Zooming in and out: scale dependence of extrinsic and intrinsic factors affecting salt marsh erosion. J. Geophys. Res. Earth Surf. 122, 1455–1470. https://doi.org/10.1002/2016JF004193.

Watson, E.B., Raposa, K.B., Carey, J.C., Wigand, C., Warren, R.S., 2017. Anthropocene survival of southern new england's salt marshes. Estuar. Coast 40, 617–625. https://doi.org/10.1007/s12237-016-0166-1.

Wrayf, R., Leatherman, S.P., Nicholls, R.J., 1995. Historic and future land loss for upland and marsh islands in the Chesapeake Bay, Maryland. U.S.A. J. Coast. Res. 11, 1195–1203.

Xiao, D., Zhang, L., Zhu, Z., 2010. The range expansion patterns of Spartina alterniflora on salt marshes in the Yangtze Estuary, China. Estuar. Coast Shelf Sci. 88, 99–104. https://doi.org/10.1016/j.ecss.2010.03.015.